JMEPEG (2008) 17:612–619
DOI: 10.1007/s11665-007-9191-3

1059-9495/$19.00

The Role of Silicon Content on Environmental Degradations of T91 Steels

A.K. Roy, D. Maitra, and P. Kumar

(Submitted August 14, 2007; in revised form November 21, 2007)

T91 grade steels showed a gradual enhancement in tensile ductility at ambient temperature due to an increase in Si content from 0.5 to 2.0 weight percent (wt.%). However, the ultimate tensile strength was reduced only above 1.5 wt.% Si. The corrosion potential became more active in an acidic solution with increasing temperature. The cracking susceptibility in a similar environment under a slow-strain-rate (SSR) condition was enhanced at higher temperatures showing reduced ductility, time to failure, and true failure stress. Cathodic potentials applied to the test specimens in SSR testing caused an enhanced cracking tendency at 30 and 60 °C, suggesting hydrogen embrittlement as a possible mechanism of failure. Cracking of precracked and wedge-loaded double-cantilever-beam specimens was enhanced at higher initial stress intensity factors. In general, steels with 2.0 wt.% Si showed inferior corrosion resistance. A combination of cleavage and intergranular brittle failure was seen in the tested specimens depending on the type of testing.

Keywords controlled potential, fractography, localized corrosion, stress corrosion cracking, stress intensity factor, T91 steels

1. Introduction

The concept of transmutation of spent nuclear fuels (SNF) has been actively pursued in recent years to enable their efficient disposal for shorter duration in the proposed geologic repository, located near Las Vegas, Nevada. Transmutation is a process of transformation of long-lived isotopes to species with shorter half-lives. Such a reduction in half-lives of SNF could lead to reduced radioactivity. The generation of neutrons involving a target material by a process, known as spallation (Ref 1), can play an important role in transmutation. This target material has to be contained inside a structural vessel made of a suitable metal or an alloy. Numerous studies (Ref 2, 3), performed at the authors' laboratories, have demonstrated that martensitic iron-chromium-molybdenum (Fe-Cr-Mo) alloys having a high silicon (Si) content may be the suitable materials to contain the target material used in the spallation process.

In view of the beneficial effect of Si previously observed (Ref 2, 3) with Fe-Cr-Mo alloys, a recent investigation was pursued to evaluate the effect of Si content on the corrosion behavior of modified 9Cr-1Mo steels, also known as T91 grade steels. The T91 grade martensitic steels have long been known to be the most suitable containment materials for nuclear applications, such as liquid-metal-fast-breeder-reactors due to the presence of niobium (Nb) and vanadium (V). Superior tensile properties, thermal conductivity, and excellent corrosion resistance have been reported (Ref 4, 5) for these alloys. However, the role of Si content on metallurgical and corrosion properties has not yet been explored by other researchers.

The beneficial effect of Si stems from the formation of protective oxide layers on the metal surface, which can promote enhanced corrosion resistance even in the presence of many aggressive chemical species (Ref 6, 7). However, the presence of unusually high Si content in these steels may exert a deleterious effect in terms of reduced ductility. Therefore, this investigation was focused on the evaluation of the corrosion behavior of martensitic T91 grade steels containing Si ranging from 0.5 to 2.0 weight percent (wt.%) in an acidic solution (pH $\sim$ 2.2) at temperatures ranging from ambient to 100 °C. Numerous state-of-the-art experimental techniques have been employed to determine the susceptibility of these materials to different types of environment-assisted degradations. Both optical microscopy and scanning electron microscopy (SEM) have also been used to characterize the morphology of failure of the tested specimens.

2. Materials and Experimental Procedures

Experimental heats of T91 grade steels containing four levels of Si were melted by a vacuum-induction-melting practice. They were subsequently forged and hot-rolled, followed by thermal treatments. All four heats were forged at 1204 °C (2200 °F) into 69.85 mm (2.75-in.) × 127 mm (5-in.) × 508 mm (20-in.) billets and air-cooled. These billets were then rolled at 1204 °C (2200 °F) into plates of different dimensions, followed by air-cooling. The thermal treatments consisted of austenitizing at 1100 °C (1850 °F) for 1 h and oil quenching. The quenched materials were subsequently tempered at 621 °C (1150 °F) for an hour, followed by air-cooling. The chemical compositions of all four heats are given in Table 1.

A.K. Roy, D. Maitra, and **P. Kumar**, Department of Mechanical Engineering, University of Nevada Las Vegas (UNLV), 4505 Maryland Parkway, Box 454027, Las Vegas, NV 89154-4027. Contact e-mail: aroy@unlv.nevada.edu.

Table 1 Chemical compositions of T91 grade steels

Heat no.	Elements, wt.%												
	C	Mn	P	S	Si	Ni	Cr	Mo	Al	V	Cb	N, ppm	Fe
2403	0.12	0.44	0.004	0.003	0.48	0.30	9.38	1.03	0.024	0.23	0.91	57	Bal
2404	0.12	0.45	0.004	0.003	1.02	0.30	9.61	1.03	0.025	0.24	0.89	53	Bal
2405	0.11	0.45	0.004	0.004	1.55	0.31	9.66	1.02	0.024	0.24	0.085	49	Bal
2406	0.11	0.45	0.004	0.004	1.88	0.31	9.57	1.01	0.029	0.24	0.087	30	Bal

Bal: Balance

Table 2 Chemical composition of test solution, g/L

Environment, pH	$CaCl_2$	K_2SO_4	$MgSO_4$	NaCl	$NaNO_3$	Na_2SO_4
Acidic (2.0-2.2)	2.77	7.58	4.95	39.97	31.53	56.74

Prior to corrosion testing, the tensile properties of all four heats of material were determined using smooth cylindrical specimens according to the ASTM Designation E 8-2004 (Ref 8). These specimens, having an overall length of 101.4 mm (4-in.), a gage-length of 25.4 mm (1-in.) and a gage-diameter of 6.35 mm (0.25-in.), were machined from the heat-treated bars in such a way that the gage-section was parallel to the longitudinal rolling direction. A similar type of specimen was also used in stress-corrosion-cracking (SCC) testing in the acidic solution involving all four heats. The composition of the testing environment is given in Table 2.

The susceptibility of these alloys to localized corrosion (pitting and crevice) was also evaluated in a similar environment using cylindrical specimens having a 12.7 mm (0.5-in.) length, a 9.5 mm (0.375-in.) diameter, and a central hole of 2.16 mm (0.085-in.) diameter for holding these specimens for electrochemical testing. Further, SCC testing was performed in an identical environment using self-loaded specimens including double-cantilever-beam (DCB), C-ring, and U-bend. The C-ring and U-bend specimens were loaded according to the ASTM Designations G 38-01 (Ref 9) and G 30-97 (Ref 10), respectively.

The rectangular DCB specimens having a 101.6 mm (4-in.) length, a 25.4 mm (1-in.) width and a 9.525 mm (0.375-in.) thickness, were used to evaluate the SCC susceptibility of all four heats of materials. These specimens were loaded by inserting double-taper wedges of different thickness into a slot, as shown in Fig. 1. V-shaped side grooves were machined on opposite sides of these specimens, extended from the slot to the opposite end to prevent branching of cracks, if any. The machining of these specimens was done according to the NACE Standard TM0177-1990 (Ref 11). The cracking susceptibility using DCB specimens was evaluated in terms of stress intensity factor (K) corresponding to different levels of load imparted by the wedges of different thickness, and the changes in crack-length.

Prior to the loading of the DCB specimens, they were precracked to an approximate length of 2 mm (0.0787-in.) in an Instron equipment according to ASTM Designation E 399-1990 (Ref 12). Cyclic loading using a load ratio (R) and frequency of 0.1 and 1 Hz, respectively, was applied to precrack these specimens. The precracked specimens were loaded to two different levels of initial stress intensity factor (K_i) by inserting wedges of two different thickness, made of a similar material. The thickness of the wedge was determined based on the displacement corresponding to the desired load within the elastic limit of the load vs. displacement (p-δ) curve, and the original gap between the two arms of the DCB specimen. The precracked and wedge-loaded DCB specimens were subsequently immersed in a 100 °C acidic solution contained in an autoclave for 30 and 60 days.

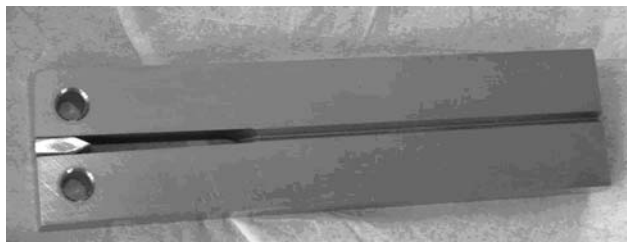

Fig. 1 Pictorial view of the DCB specimen

Upon completion of testing, the final load imparted by the wedge was determined from the elastic region of the p-δ curve generated on the tested specimen, which was subsequently broken apart under tensile loading to determine the crack extension on its broken surfaces. SEM was used to determine the crack-extension resulting from the combined effect of the wedge-load and the testing environment. The final stress intensity factor (K_f) was calculated using the final load and crack length. The magnitudes of K_i and K_f were computed using the following equation. The detailed experimental procedure for the determination of the cracking susceptibility of T91 grade steels using DCB specimens has been described in a recent publication (Ref 13).

$$K = \frac{Pa\left(2\sqrt{3} + 2.38h/a\right)(B/B_n)^{1/\sqrt{3}}}{Bh^{3/2}}$$

where,

P = Wedge load (before or after exposure to the environment), measured in the loading plane (N);
a = The initial or final crack length, measured from the load line (m);
h = The height of each arm (m);
B = The specimen thickness (m);
B_n = The web thickness (m).

The SCC testing using smooth cylindrical specimens of all four heats of T91 grade steel was performed under both constant-load (CL) and slow-strain-rate (SSR) conditions. For CL testing, these specimens were loaded in tension using an applied load corresponding to 95% of the materials' room

temperature yield strength (YS) values. A strain-rate of 3.3×10^{-6} s^{-1} was used in the SSR testing to optimize the combined effect of the applied stress and the testing environment to promote SCC. The SCC susceptibility at CL was expressed as the threshold stress (σ_{th}), below which cracking did not occur in 30 days in the presence of the acidic solution. The SCC behavior under the SSR condition was measured in terms of the time-to-failure (TTF), the true failure stress (σ_f), and ductility parameters including the percent elongation (%El) and the percent reduction in area (%RA). The experimental procedures associated with both constant load and SSR testing methods have been given elsewhere (Ref 14-16).

The susceptibility of the tested materials to localized corrosion was determined using the cyclic potentiodynamic polarization (CPP) method. This technique was based on a three-electrode polarization principle, in which the working electrode (test specimen) acted as an anode, two graphite electrodes acted as cathodes, and the reference electrode was made of silver/silver chloride (Ag/AgCl) solution contained inside a Luggin probe. Prior to the CPP experiments, the potentiostat was calibrated according to the ASTM Designation G 5 (Ref 17). Finally, the susceptibility of T91 grade steels to SCC was determined under controlled cathodic and anodic potentials (E_{cont}) using the SSR technique. The magnitudes of E_{cont} were based on the corrosion potential (E_{corr}) determined from the CPP experiments, as described in several recent publications (Ref 14-16).

The metallurgical microstructures, and the morphology of failures of the tested specimens were evaluated using optical microscopy and SEM, respectively. A metallographic montage of a broken DCB specimen was also developed based on the optical micrographs developed at different regions corresponding to precracking by cyclic loading, SCC and fast fracture, respectively. The C-ring and U-bend specimens were also examined by optical microscopy and SEM to detect cracking on the curved surfaces, if any.

3. Results and Discussion

The optical micrographs of the polished and etched specimens of T91 grade steels in the heat-treated condition are illustrated in Fig. 2, as a function of the Si content. These micrographs revealed that the grain size became finer with increasing Si content, while showing predominantly tempered martensitic microstructures. However, elongated streaks of martensite were seen in the tempered martensitic matrix of steel having 1.0 and 1.5 wt.% Si. The morphology of the martensitic streaks was changed to irregular shapes in steel containing 2.0 wt.% Si. The presence of ferrite (dark spots) was seen in all micrographs, irrespective of the Si content.

The results of room-temperature tensile testing involving all four heats of steels are illustrated in Fig. 3 in the form of superimposed engineering stress vs. engineering strain (s-e) diagram. The magnitude of the YS, ultimate tensile strength (UTS), %El and %RA, derived from these s-e diagrams and the specimen dimensions, are given in Table 3. These data indicate that the magnitude of YS was not influenced by the changes in Si content up to 1.5 wt.%. However, the UTS was slightly enhanced with an increase in Si content from 0.5 to 1.5 wt.%. The tensile strength in terms of both YS and UTS was reduced to some extent in steel containing 2.0 wt.% Si. The slightly enhanced tensile strength in terms of UTS in steels containing 0.5-1.5 wt.% Si could be the result of precipitation of Si near the ferrite phase, as suggested by several investigators (Ref 18, 19). Such precipitation of Si around the ferrite phase could impede the dislocation motion, thus, leading to work-hardening of these steels.

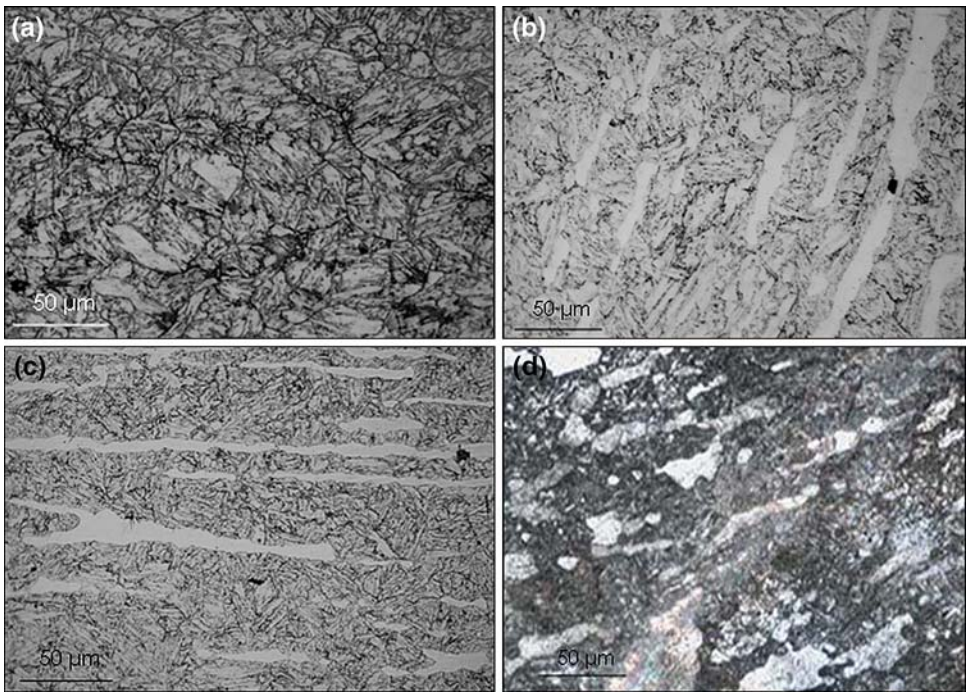

Fig. 2 Optical micrographs of T91 grade steel, Beraha's Reagent, 500×. (a) 0.5 wt.% Si (b) 1.0 wt.% Si (c) 1.5 wt.% Si (d) 2.0 wt.% Si

The addition of higher Si content (2.0 wt.%) in a T91 grade steel may reduce the carbon (C) and nitrogen (N) levels near grain boundaries, which could have caused the softening of the martensitic matrix instead of hardening, as cited in the open literature (Ref 20). Nevertheless, the ductility of all four steels was gradually enhanced in terms of %El and %RA with increasing Si content. The enhanced ductility with increasing Si content could be attributed to the increased uniform plastic strain up to the point of instability (necking) (Ref 21).

The results of localized corrosion study using the CPP technique indicates that all the four heats of material exhibited an active to passive transition, showing both corrosion potential (E_{corr}) and critical pitting potential (E_{pit}), when tested in the 30 °C acidic solution. However, at 60 and 90 °C, the CPP diagrams of all tested materials exhibited an active behavior alone, implying rapid dissolution at elevated temperatures. The CPP diagrams of T91 grade steel with 1.0 wt.% Si, obtained in 30 and 90 °C acidic solution are illustrated in Fig. 4, showing an active to passive, and an active behavior only, respectively.

The magnitudes of E_{corr} and E_{pit}, if any, determined from the CPP diagrams are given in Table 4. The variations of E_{corr} with temperature for steels of different Si content are illustrated in Fig. 5. These data clearly indicate that the magnitude of E_{corr} became more active (negative) with increasing temperature due to enhanced dissolution at elevated temperatures. A similar observation on the detrimental effect of higher temperature on E_{corr} has been reported by other investigators (Ref 22). As to the effect of Si content on E_{corr}, its value became more noble with an increase in Si content from 0.5 to 1.5 wt.%, irrespective of the testing temperatures. However, at 2.0 wt.% Si, E_{corr} became slightly more active, indicating relatively higher dissolution due to the presence of increased Si content. Interestingly, none of the polarized specimens did exhibit any pitting or crevice corrosion on their surfaces.

Stress-corrosion-cracking testing performed at constant load involving all four heats of material did not exhibit any cracking in the acidic solution, irrespective of the testing temperature. These data might indicate a σ_{th} value equivalent to 0.95YS of each material, when tested in an acidic environment. As to the SCC susceptibility in a similar solution under a SSR condition, a gradual reduction in failure strain (e_f) was observed in the superimposed s-e diagrams for all four materials with increasing temperature. The effect of temperature on e_f for steel containing 0.5 wt.% Si is illustrated in Fig. 6.

Similarly, the magnitudes of TTF, σ_f, %El, and %RA were gradually reduced at higher temperatures (Table 5), implying a detrimental effect of higher temperatures on the cracking susceptibility of Si-containing martensitic alloys. It is, however, interesting to note that the enhanced cracking tendency in the 90 °C acidic solution was more pronounced in steel containing

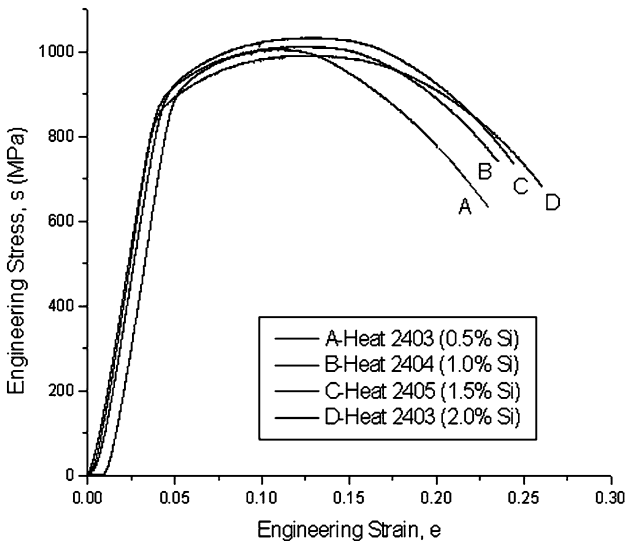

Fig. 3 Superimposed s-e diagrams vs. Si content

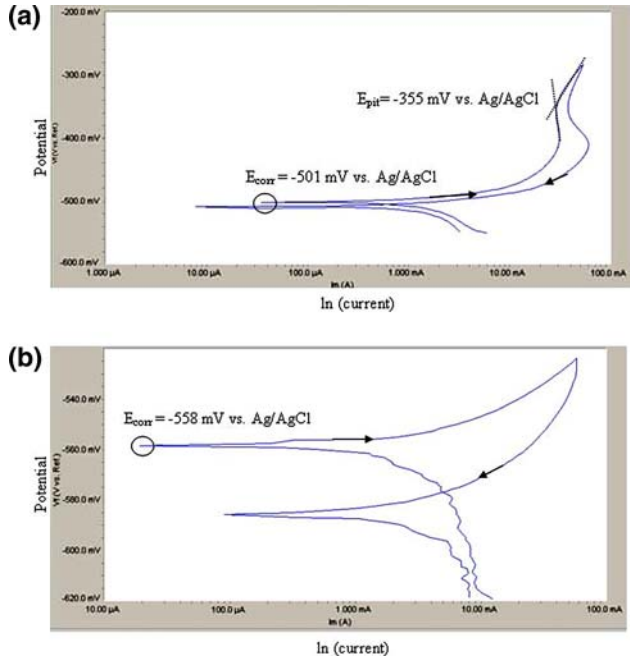

Fig. 4 (a) CPP diagram in 30 °C acidic solution (1.0 wt.% Si). (b) CPP diagram in 90 °C acidic solution (1.0 wt.% Si)

Table 3 Tensile data vs. Si content

	YS, MPa, ksi			UTS, MPa, ksi			%El			%RA		
Heat no./Si content	**Test 1**	**Test 2**	**Av.**	**Test 1**	**Test 2**	**Av.**	**Test 1**	**Test 2**	**Av.**	**Test 1**	**Test 2**	**Av.**
2403/0.5% Si	889 (129)	883 (128)	889 (129)	1007 (146)	1007 (146)	1007 (146)	23.1	23.5	23.3	59.7	60.3	60.0
2404/1.0% Si	883 (128)	889 (129)	889 (129)	1007 (146)	1014 (147)	1014 (147)	23.8	23.2	23.5	62.3	61.7	62.0
2405/1.5% Si	889 (129)	889 (129)	889 (129)	1027 (149)	1027 (149)	1027 (149)	24.2	24.6	24.4	71.0	69.9	71.0
2406/2.0% Si	841 (122)	848 (123)	848 (123)	993 (144)	993 (144)	993 (144)	26.1	25.9	26.0	76.0	76.2	76.1

1 ksi = 6.895 MPa
Av. = Average value

Table 4 Results of CPP testing in acidic solution

Temperature, °C	0.5 wt.% Si		1.0 wt.% Si		1.5 wt.% Si		2.0 wt.% Si	
	E_{corr}, mV (Ag/AgCl)	E_{pit}, mV (Ag/AgCl)	E_{corr}, mV (Ag/AgCl)	E_{pit}, mV (Ag/AgCl)	E_{corr}, mV (Ag/AgCl)	E_{pit}, mV (Ag/AgCl)	E_{corr}, mV (Ag/AgCl)	E_{pit}, mV (Ag/AgCl)
30	−506	−360	−501	−355	−495	−350	−511	−100
60	−553	None	−553	None	−547	None	−550	None
90	−561	None	−558	None	−550	None	−563	None

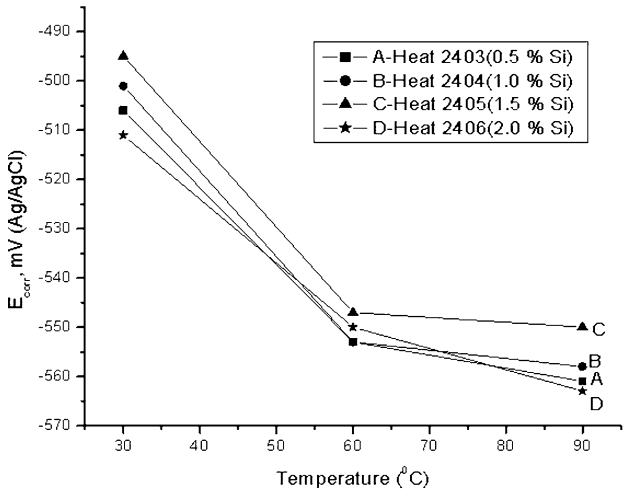

Fig. 5 Variation of E_{corr} with temperature as a function of Si content

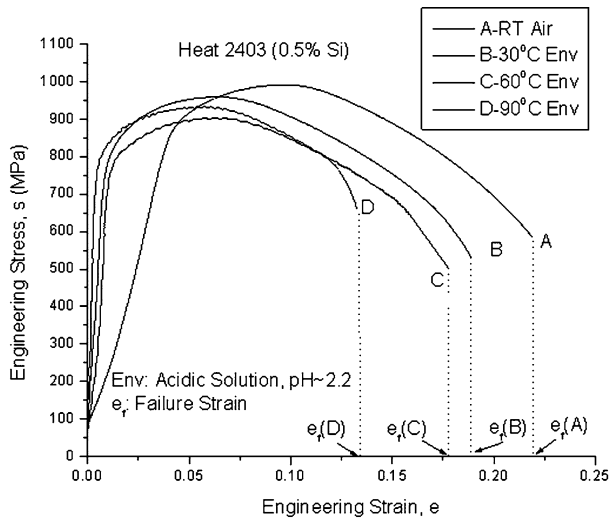

Fig. 6 s-e Diagram vs. environment and temperature

Table 5 Results of SSR testing

Heat no./Si content	Temperature, °C, environment	%El	%RA	TTF, h	σ_f, MPa, ksi
2403/0.5% Si	RT, Air	21.9	62.0	19.5	910 (132)
	30, AS	18.9	35.0	18.8	814 (118)
	60, AS	17.7	33.6	16.9	800 (116)
	90, AS	13.3	28.5	15.1	765 (111)
2404/1.0% Si	RT, Air	24.8	64.5	20.1	917 (133)
	30, AS	19.0	35.0	19.0	807 (117)
	60, AS	17.7	33.5	17.0	793 (115)
	90, AS	13.2	28.2	14.9	765 (111)
2405/1.5% Si	RT, Air	25.7	71.6	20.8	917 (133)
	30, AS	19.0	35.0	19.2	807 (117)
	60, AS	17.5	33.5	17.0	793 (115)
	90, AS	13.1	28.3	14.8	758 (110)
2406/2.0% Si	RT, Air	28.0	76.0	24.1	931 (135)
	30, AS	23.5	42.0	21.7	834 (121)
	60, AS	18.0	36.3	17.6	807 (117)
	90, AS	10.1	24.0	13.7	676 (98)

AS: Acidic solution, pH ~ 2.2

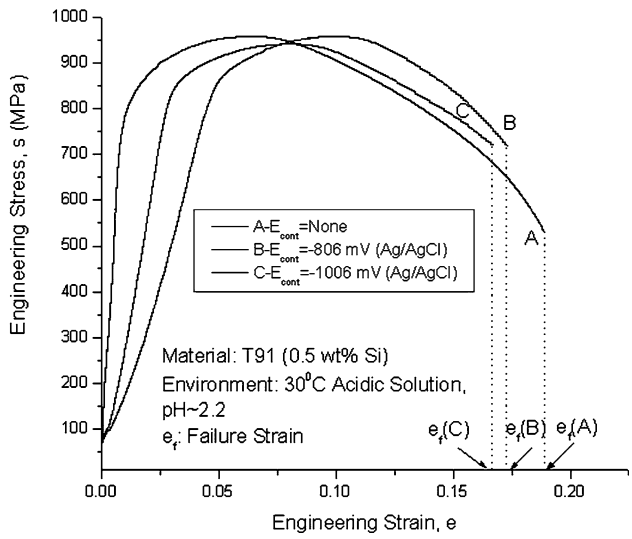

Fig. 7 s-e Diagram vs. cathodic E_{cont}

2.0 wt.% Si. A similar observation as to the role of temperature on the SCC susceptibility of Cr-Mo steels in acidic solutions has been reported by several investigators (Ref 3, 16).

The results of SSR testing under a potentiostatic control indicate that the application of cathodic (negative vs. E_{corr}) E_{cont} resulted in enhanced susceptibility to SCC of all tested materials at 30 and 60 °C. The detrimental effect of cathodic E_{cont} on e_f is illustrated in Fig. 7 for a T91 grade steel containing 0.5 wt.% Si. The enhanced cracking tendency in terms of reduced e_f may be attributed to the diffusion of hydrogen generated from cathodic charging at these temperatures under a potentiostatic control, and subsequent entrapment of hydrogen inside the matrix of the tested materials (Ref 23). At 90 °C, the effect of cathodic applied potential on the

cracking susceptibility was minimal possibly due to permeation of generated hydrogen through the matrix of the tested material, as cited in the open literature (Ref 19). Interestingly, the application of anodic E_{cont} did not adversely influence the cracking tendency of the tested materials in the 30 and 90 °C acidic solutions, suggesting that hydrogen-embrittlement may be the plausible mechanism of cracking for Si-containing martensitic steels tested in this investigation.

The result of SCC testing using precracked and wedge-loaded DCB specimens are given in Table 6. These results indicate that the magnitudes of crack-extension (Δa) and the reduction in stress intensity factor (ΔK), upon completion of testing for desired durations, were pronounced in specimens loaded to higher K_i values. Further, the load imparted by the wedge was dropped substantially at the conclusion of testing. Such reduction in wedge-load resulted in reduced K_f values. As to the effect of Si content on K, the magnitude of ΔK was maximum for steel containing 2.0 wt.% Si. The detrimental effect of Si above 1.5 wt.% has also been noted in SCC testing in the 90 °C acidic solution using the SSR method.

An evaluation of the tested C-ring and U-bend specimens of all heats of material indicates that no cracks were observed along the thickness of these specimens. However, a combination of general dissolution and tiny cracks was seen in the optical micrographs at the convex surface of these specimens. The extent of damage on the convex surface was, however, more pronounced in the C-ring specimens. The presence of tiny cracks in these specimens was more frequent in steels containing Si up to 1.5 wt.%. General dissolution was, however, seen on the surface of the C-ring specimens containing 2.0 wt.% Si. The evaluation of the C-ring specimens by SEM revealed intergranular cracking on their convex surfaces irrespective of the Si content, as shown in Fig. 8.

The evaluations of the primary fracture surface of the tested tensile specimens revealed a combination of cleavage and intergranular failures. Similar types of failure were seen in the cylindrical specimens used in the SSR testing. However, the fracture morphology of the specimens tested at 90 °C was characterized by severe intergranular cracking, as shown in Fig. 9. These results, once again, imply that the cracking susceptibility was more pronounced at 90 °C in the presence of the acidic solution. The SEM micrographs of a broken DCB specimen of steel with 0.5 wt.% Si are illustrated in Fig. 10, showing three regions of failure corresponding to cyclic loading, SCC and fast fracture. These micrographs were used to estimate the final crack length (a_f) of the DCB specimens, resulting from the combined effect of precracking at the notch and SCC.

Table 6 Results of DCB testing

Heat no./Si content	Initial wedge load, N	Final wedge load, N	a_i, m	a_f, m	Δa, m	K_i, MPa√m	K_f, MPa√m	ΔK, MPa√m	Test duration, days	CGR, m/h
2403/0.5 wt.% Si	2669	2157	0.034	0.042	0.008	38.70	37.17	1.53	60	55.6×10^{-7}
	4003	3114	0.034	0.043	0.009	58.04	54.71	3.33	30	124.9×10^{-7}
2404/1.0 wt.% Si	3559	3025	0.034	0.040	0.006	51.59	50.05	1.54	60	41.7×10^{-7}
	5338	4359	0.034	0.041	0.007	77.38	73.61	3.77	60	48.5×10^{-7}
2405/1.5 wt.% Si	4448	3781	0.034	0.040	0.006	64.49	62.56	1.93	60	41.7×10^{-7}
	6228	4671	0.034	0.045	0.009	90.28	86.47	3.81	30	131.6×10^{-7}
2406/2.0 wt.% Si	3559	2891	0.034	0.040	0.006	51.59	47.27	4.32	30	83.3×10^{-7}
	5338	4003	0.034	0.042	0.008	77.38	68.97	8.41	60	55.6×10^{-7}

a_i = Initial crack length
a_f = Final crack length
Δa = Change in crack length
K_i = Initial stress intensity factor
K_f = Final stress intensity factor
ΔK = Change in stress intensity factor
CGR = Overall crack growth rate

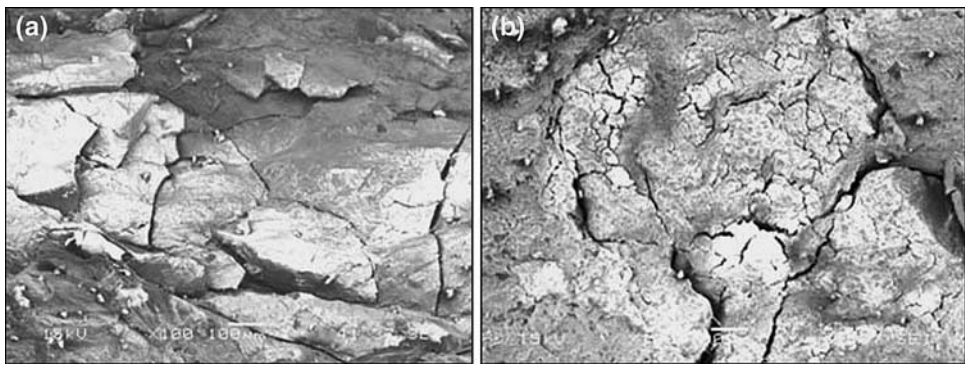

Fig. 8 SEM micrographs of convex surfaces of C-ring specimens. (a) 0.5 wt.% Si, 60 days, 100× (b) 2.0 wt.% Si, 60 days, 100×

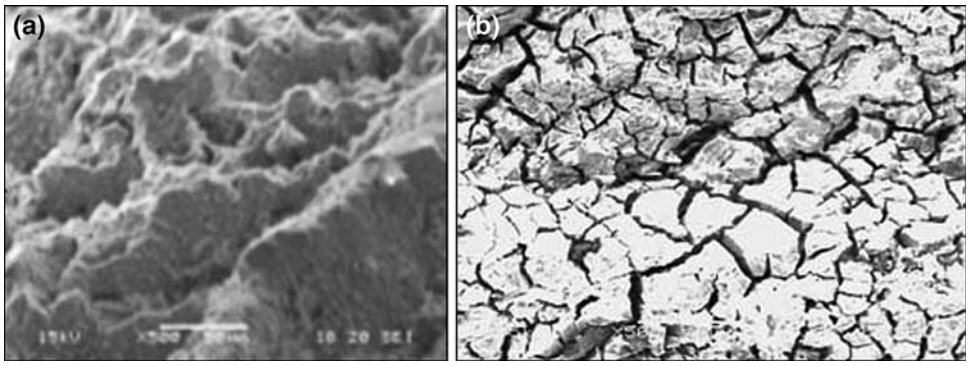

Fig. 9 SEM micrographs of primary fracture surface of SSR specimens, 500×. (a) 1.0 wt.% Si, RT, air (b) 1.0 wt.% Si, 90 °C, aqueous solution

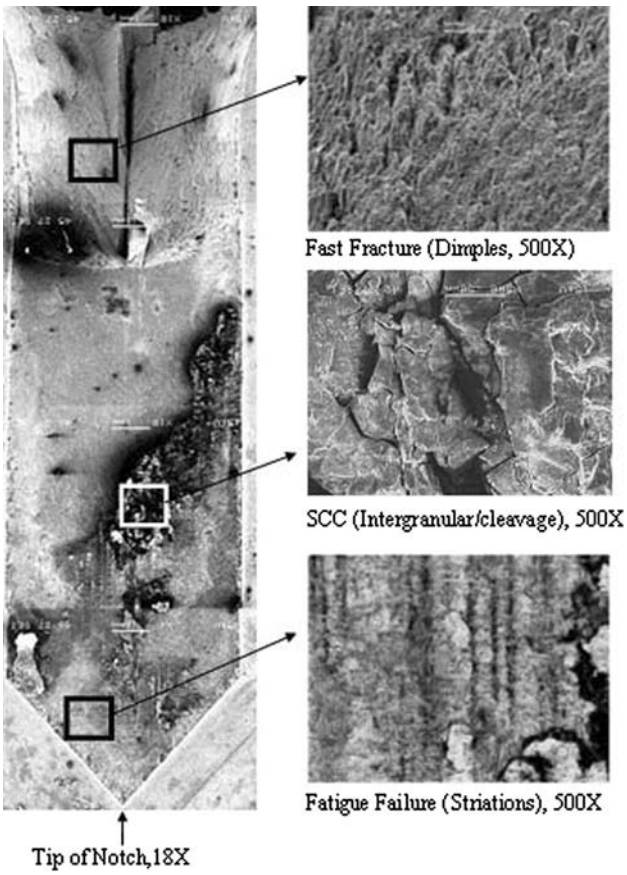

Fig. 10 Fracture morphology at different regions of a broken DCB specimen

4. Summary and Conclusions

Martensitic T91 grade steels of varying Si content were tested for evaluation of their room-temperature tensile properties, susceptibility to SCC, and localized corrosion behavior in an acidic solution at ambient and elevated temperatures. The role of controlled anodic and cathodic potentials (E_{cont}) on their SCC susceptibility was also investigated. Microstructural and fractographic evaluations of the tested specimens were performed by optical microscopy and SEM, respectively. The key results and the significant conclusions drawn from this investigation are summarized below:

- The optical micrographs revealed finer tempered martensitic microstructure with increasing Si content.
- Slight enhancement in tensile strength in terms of UTS was observed in steels containing 0.5-1.5 wt.% Si that could be the result of work-hardening. At 2.0 wt.% Si, the UTS was reduced possibly due to the reduction in C and N levels, causing softening of the martensitic matrix.
- The plastic strain up to necking was gradually enhanced with increasing Si content, showing improved ductility.
- The magnitude of E_{corr} became more active with increasing temperature. At elevated temperatures, no active to passive transition was observed with any tested materials.
- T91 grade steels exhibited gradual ennoblement of E_{corr} values due to the presence of Si up to 1.5 wt.%, irrespective of the testing temperature.
- A σ_{th} value of 0.95YS was estimated from the SCC testing in the acidic solution at constant load.
- The SCC susceptibility in a similar environment was gradually enhanced with increasing temperature under a SSR condition, showing reduced %El, %RA, TTF and σ_f. As to the Si effect, steel with 2.0 wt.% Si showed maximum cracking tendency in terms of these parameters at 90 °C.
- The cracking tendency under cathodic E_{cont} values was more pronounced at 30 and 60 °C due to the generation and entrapment of hydrogen within the metal matrix. However, no adverse effect of anodic E_{cont} on cracking was observed.
- The susceptibility of steels to SCC in terms of K_f was more pronounced in DCB specimens loaded to higher K_i values.
- The primary fracture surface of the cylindrical tensile and SSR specimens, evaluated by SEM, was characterized by a combination of cleavage and intergranular failures. The SEM micrographs of the C-ring specimens revealed intergranular attack at their convex surfaces.

Acknowledgment

This work was funded by the United States Department of Energy under grant number DE-FC07-06 ID14781.

References

1. F. Venneri, M.A. Williamson, N. Li, M.G. Houts, R.A. Morley, D.E. Beller, W. Sailor, and G. Lawrence, Disposition of Nuclear Waste using Subcritical Accelerator-Driven Systems: Technology Choices and Implementation Scenarios, *Nucl. Technol.*, 2000, **132**, p 15
2. A.K. Roy and M.K. Hossain, Environment-Assisted Cracking of Structural Materials Under Different Loading Conditions, *Corrosion*, 2005, **61**(4), p 364
3. A.K. Roy and M.K. Hossain, Cracking of Martensitic Alloy EP-823 Under Controlled Potential, *J. Mater. Eng. Perform.*, 2006, **15**(3), p 336
4. T. Hayashi, M. Takamoto, K. Ito, and K. Tanaka, The Effect of Nb and W Alloying Additions to the Thermal Expansion Anisotropy and Elastic Properties of Mo_5Si_3, *Met. Mat. Tran.*, 2005, **36A**(3), p 533
5. J.L. Boutard, Y. Dai, and K. Ehrlich, MEGAPIE General Meeting
6. A.M. Huntz, V. Bague, G. Beauplé, C. Haut, C. Sévérac, P. Lecour, X. Longaygue, and F. Ropital, Effect of Silicon on the Oxidation Resistance of 9% Cr Steels, *Appl. Surf. Sci.*, 2003, **207**(1–4), p 255
7. R. Nishimura, K. Yamakawa, and J. Ishiga, Highly Corrosion Resistant Stainless Steel with Si Implanted/Deposited Phase, *Mat. Chem. Phys.*, 1998, **54**(1–3), p 289
8. ASTM Designation E 8-2004, Standard Test Methods for Tensile Testing of Metallic Materials, American Society for Testing and Materials (ASTM) International, 2004
9. ASTM Designation G 38, Standard Practice for Making and Using C-Ring Stress-Corrosion Test Specimens, American Society for Testing and Materials (ASTM) International, 2001
10. ASTM Designation G 30, Standard Practice for Making and Using U-Bend Stress-Corrosion Test Specimens, American Society for Testing and Materials (ASTM) International, 1997
11. NACE Standard TM0177, Laboratory Testing of Metals for Resistance to Sulfide Cracking in H_2S Environments, National Association of Corrosion Engineers (NACE), 1990, p 16
12. ASTM Designation E 399, Standard Test Method for Linear-Elastic Plain-Strain Fracture Toughness K_{1C} of Metallic Materials, American Society for Testing and Materials (ASTM) International, 1999
13. D. Maitra, Tensile Deformation and Environmental Degradation of T91 Grade Steels with Different Silicon Content, PhD Dissertation, Mech. Eng., UNLV (2007)
14. A.K. Roy and V. Virupaksha, Performance of Alloy 800H for High-Temperature Heat Exchanger Applications, *Mat. Sci. Eng. A*, 2007, **452–453**, p 665
15. A.K. Roy and A.V. Kaiparambil, Tensile and Corrosion Behavior of Zr705 for Nuclear Hydrogen Generation, *Mat. Sci. Eng. A*, 2006, **427**, p 320
16. R. Prabhakaran and A.K. Roy, Degradations of Type 422 Stainless Steel in Aqueous Environments, *Mat. Sci. Eng. A*, 2006, **421**, p 290
17. ASTM G 5-94, Standard Reference Test Method for Making Potentiostatic and Potentiodynamic Anodic Polarization Measurements, American Society for Testing and Materials (ASTM) International, 1999
18. B.V.N. Rao and M.S. Rashid, Direct Observations of Deformation-Induced Retained Austenite Transformation in a Vanadium-Containing Dual-Phase Steel, *Metallography*, 1983, **16**, p 19
19. L.C. Covington, The Influence of Surface Condition and Environment on the Hydriding of Titanium, *Corrosion*, 1979, **35**(8), p 378
20. B. Mintz, Role of Silicon in Influencing Strength and Impact Behavior of Ferrite and its Likely Influence at Ultrafine Grain Size, *Struc. Mat. Mat. Cong.*, 2000, **16**, p 1282
21. J.M. Rigsbee and P.J. Vanderarend, *Formable HSLA and Dual-Phase Steels*, New York, TMS-AIME, 1977, p 56
22. A.K. Roy, D.L. Fleming, and B.Y. Lum, Localized Corrosion Behavior of Candidate Nuclear Waste Package Container Materials, *Mat. Perform.*, 1998, **37**, p 54
23. I. Azkarate, A. Pelayo, and L. Victori, *Progress in the Understanding and Prevention of Corrosion*, vol. 2, 1993, p 1573